AIMS Energy, 9(6): 1147–1169.
DOI: 10.3934/energy.2021053
Received: 18 August 2021
Accepted: 08 November 2021
Published: 18 November 2021

http://www.aimspress.com/journal/energy

Research article

Parametric design analysis of elliptical shroud profile

Salih Nawaf Akour* and Mahmoud Azmi Abo Mhaisen

Mechanical Engineering Department, School of Engineering, The University of Jordan

* **Correspondence:** Email: akour@ju.edu.jo; Tel: +9626535000.

Abstract: Parametric design analysis for Eccentric Rotated Ellipsoid (ERE) shroud profile is conducted whereas the design model is validated experimentally. A relation between shroud inlet, length and exit diameter is established, different ratios related to the wind turbine diameter are introduced, and solution for different ERE family curves that passes on the inlet, throat, and exit points is studied. The performance of the ERE shroud is studied under different wind velocities ranging from 5–10 m/s.

The method used in creating the shroud profile is by solving the ERE curve equations to generate large family of solutions. The system is modeled as axisymmetric system utilizing commercial software package. The effect of the parameters; shroud length, exit diameter, inlet diameter, turbine position with respect to the shroud throat, and wind velocity are studied. An optimum case for each shroud length, exit diameter and location of the shroud with respect to the wind turbine throat axis are achieved.

The simulation results show an increase in the average wind velocity by 1.63 times of the inlet velocity. This leads to a great improvement in the wind turbine output power by 4.3 times of bare turbine. One of the achieved optimum solutions for the shroud curves has been prototyped for experimental validation. The prototype has been manufactured using 3D printing technology which provides high accuracy in building the exact shape of shroud design curve. The results show very good agreement with the experimental results.

Keywords: wind energy; wind lens; elliptic shroud; low wind speed regions

1. Introduction

Increasing the power harvested by wind turbines attracted the attention of many researchers worldwide. Some turbines are augmented by diffusers whereas others are augmented by shrouds. Through investigations for equipping wind turbines with diffusers can be found in references [1–7]. Diffuser equipped with a flange is known as shroud. Compact shrouds are called wind lens i.e., the width of the shroud is small compared to its diameter. In small size wind turbine, the addition of shroud to a bare wind turbine increases the power output in significant amount. The reason for this increment is the behavior of the flow inside and outside existence the shroud that leads to an increase in the air velocity inside the shroud, furthermore this increases the power output of the wind turbine. The most dominant behavior of the flow around the shroud is the formation of the vortices that contributes to the behavior of the flow inside and outside the shroud. The shape of the shroud plays the main role in sizing vortices formed behind the shroud exit.

Shroud design still needs more development and research, because no optimum shape for the inlet, body and exit of the shroud is found. Also, no optimum geometrical shape was developed linking these three parts together into one blended part. The shroud design based on airflow and vortices formation needs to be investigated.

The shroud body (diffuser shape) has an outlet size larger than its inlet (shroud throat). The wind velocity in the diffuser part accelerates instead of known phenomena of deceleration in diffusers due to vortices generation behind the body exit. The vortices generation occurs due to low-pressure regions formed due to turbulent flow. This turbulence formed when separation at shroud inner and outer surfaces take place.

The shroud exit is equipped in many previous studies by means of a flange with different shapes and tilting angles. Such flange acts as an amplifier for the vortices generation. It increases the length of the flow separation that occurs at the shroud inner and outer surfaces, and changes the flow direction just before the exit at the shroud outer surface.

Recently Ohya et al. studied shrouded axial wind turbine. Their results showed that the shrouded wind turbine equipped with a flanged diffuser demonstrated power augmentation by a factor of about 4–5 times compared to a standard bare wind turbine. In addition, a field experiment using a prototype wind turbine with a flanged diffuser shroud was conducted. The output performance was as expected and was in agreement with that of the wind tunnel experiment [8].

Ohya and Karasudani (2010) developed a wind turbine with a compact diffuser shroud. Different profiles with different section shapes were compared. The compact shroud (wind lens) turbine demonstrated power augmentation by a factor of up to 2.5 times compared with a bare wind turbine of 5 kW power output. They used a length to diameter ratio of 0.221–0.225 with different profile shapes, and the rotor diameter (D) of the wind turbine was 2.5 meters with a flange height of 0.1 D [9].

Srikanth et al. (2007) analyzed 2D axisymmetric model and studied the velocity development inside the shroud. Their results showed increase in wind stream velocity twice as maximum and 1.5 as average near the rotor [10]. Takahashi et al. (2012) conducted 3D numerical simulation and found that the flow around turbine is complex and unsteady. The formation of vortices behind the shroud exit clearly appeared [11]. Kosasih and Tondelli (2012) carried out CFD simulation for AMPAIR 300 wind turbine and achieved 41% increase in power output. Maximum Cp achieved for bare wind turbine was 0.257, and for shrouded wind turbine was 0.31 [12]. Toshimitsu et al. (2012)

investigated the effect of actual sinusoidal oscillating and fluctuating flow of wind. Their results showed that the shrouded wind turbine had higher efficiency than bare wind turbine for both steady and unsteady wind [13]. Govindharajan et al. (2013) investigate different shroud profiles and obtained 23–35% increase in air mass flowrate inside the shroud [14]. Jafari and Kosasih (2014) carried out CFD analysis for different shapes of shroud, they found that the back pressure behind the shroud is the most influential factor in power increment [15]. Kosasih and Jafari (2014) carried out CFD simulation for AMPAIR 300 wind turbine and achieved 41% increase in power output. Maximum C_p achieved for bare wind turbine was 0.257, and for shrouded wind turbine was 0.31 [16]. Maia (2014) performed numerical and experimental analysis for shrouded wind turbine, the experimental results show increase of 90% in the output power [17]. Sangoor (2015) performed numerical and experimental analysis for shrouded wind turbine and achieved increase of 1.7–2.3 times in the power output [18]. Liu et al. (2016) use axisymmetric analysis in CFD. Their results showed increase of 50% in velocity and decrease of 49% in drag force inside the shroud [19]. Jenkins et al. (2016) presented a numerical flow simulation for large scale shrouded wind turbine. Their model was impractical due to difficulties in design [20]. Oka et al. (2016) developed shrouded wind turbine based on quasi 3D aerodynamic design method. Their results showed that Betz limit can be exceeded in shrouded wind turbines [21]. El-Zahaby et al. (2017) analyzed flanged shroud using 2D axisymmetric CFD model. They obtained numerical increase in power output of 1.7 time the bare wind turbine. They studied the flange tilt angle and found that 5% increase is achieved at +15° compared to right angle flange [22]. Ohya et al. (2017) developed 10 kW hexagonal shrouded wind turbine consisting of multi shrouded wind turbine of size 3 kW [23].

From previous studies on wind lens turbine shrouds, it can be concluded that the shroud design starts with a combined shape comprising an inlet, shroud body, and exit. In some cases, flange was added at the shroud end to increase the power of the wind turbine.

In most of the previous studies the shroud inlet, body, and exit were studied as separate parts and then combining them into one complete geometry. Some cases try to solve the shroud geometry in terms of polynomial equation, to combine the geometry parts of the shroud in analytical equation. This type of development on the shroud geometry shows that the shroud geometry can be developed analytically as well as experimentally.

1.1. Objective of present research

This study aims to design and analyze Eccentric Rotated Ellipsoid (ERE) shroud as one blended geometry. This unique profile connects the inlet, body, and exit of the shroud in one profile. A set of elliptical profiles is going to be generated. Comparison among these profiles will be carried out to find the best performance profile. The shroud will be modeled as axisymmetric system utilizing an in-house ANSYS Software package. Different design parameters will be investigated to reach the optimum ones such as inlet diameter, throat diameter, exit diameter, body length, and inlet length.

Experimental validation is conducted to validate simulation results. The experimental model is implemented utilizing 3D printing technology.

1.2. Problem statement

Shroud option for small wind turbines makes it an attractive choice for urban use, where a couple of shroud wind turbines can cover ordinary home power demand. It can also be used in a hybrid system incorporating solar systems. This is a good option for users in Jordan as well as worldwide of similar climate.

2. Physical, mathematical and simulation models

The following subsections present the details of the physical, mathematical and simulation models.

2.1. Physical model

The general shape of the shroud based on some previous studies was assumed to consist of three main parts; the inlet, the shroud body, and the exit. The inlet section which lies in front of the turbine blades axis is called the mouth. It has an inlet size larger than its outlet at the shroud throat. It acts as a nozzle to accelerate the wind stream entering the turbine blades section. The shroud body is chosen to be ERE that forms blended geometry which includes all the three parts together in one profile, i.e., the parts are linked together by one mathematical equation. The assumptions of the shroud geometrical parameters are:

1. The Shroud Inlet Diameter, D_i.
2. The Shroud Exit Diameter, D_e.
3. The Mouth Length which is the distance between the shroud inlet and the throat at which the wind turbine blades are located, L_i.
4. The Shroud Body Length L_b.
5. The Wind Turbine Diameter D_{wt}.
6. The Clearance c which is the distance between the wind turbine blades tip and the shroud inner surface at the throat. The clearance should be as minimum as possible to utilize the wind stream acceleration near the shroud at the throat.
7. To link the shroud geometry variables with respect to the wind turbine diameter, the concept of Total Throat Diameter D_{th} will be defined. The total diameter at throat D_{th} is:

$$D_{th} = D_{wt} + 2c \tag{1}$$

From the above assumptions made for the shape of the designed shroud curve, the general shape of the shroud is shown in Figure 1.

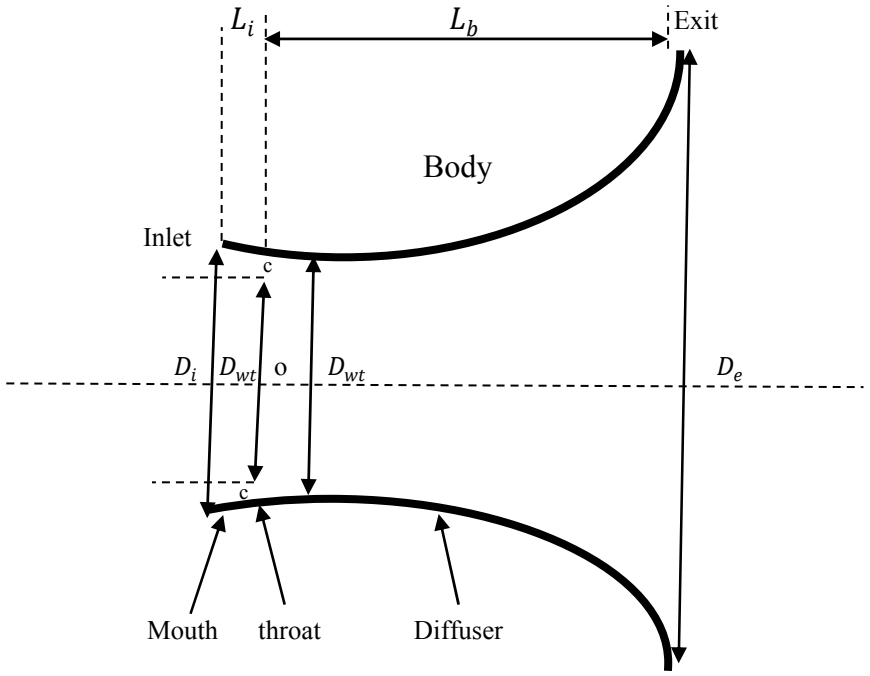

Figure 1. Shroud parts and design parameters.

In order to generalize the study, the parameters are introduced in dimensionless format by relating them to the throat diameter as the following:

1. Ratio A_1 is the Shroud Inlet Diameter and Total Throat Diameter $A_1 = \frac{D_i}{D_{th}}$
2. Ratio A_2 is the Shroud Exit Diameter and Total Throat Diameter $A_2 = \frac{D_e}{D_{th}}$
3. Ratio A_3 is the Mouth Length and Total Throat Diameter $A_3 = \frac{L_i}{D_{th}}$
4. Ratio A_4 is the Body Length and Total Throat Diameter $A_4 = \frac{L_b}{D_{th}}$

2.1.1. Shroud geometrical equations

In order to develop mathematical relation for 2D geometry, the locations of inlet, throat, and exit are assumed as points on 2D plane. The origin point of the elliptical shroud is assumed to be the intersection between the turbine shaft axis and the turbine blades axis (throat axis). Three points lying on the designed shroud curve are obtained namely, the inlet, throat, and exit points. These three points establish a reference for the design analysis; where the shroud curve equations must satisfy these three points as shown in Figure 2.

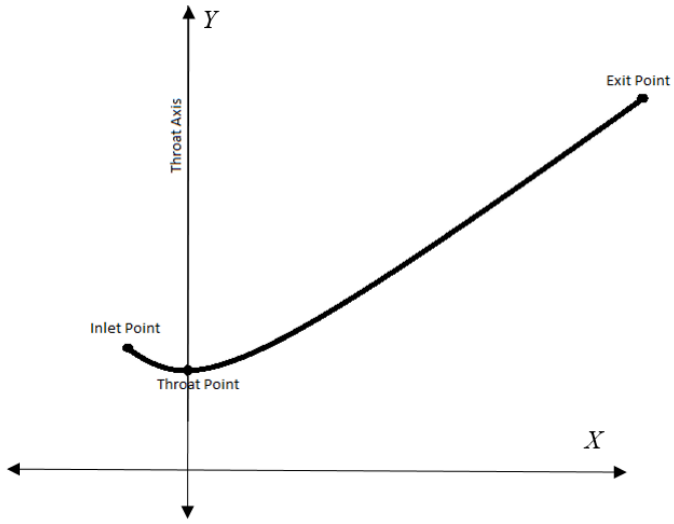

Figure 2. Simple shroud curve diagram.

2.1.2. Initial assumptions for design variables

The shroud exit diameter and shroud body length of initial assumption for geometry in this research, has been chosen close to the profiles studied by Ohya et al. [9]. But in their analysis of compact wind lens profile, they used flanged diffuser which is quite different from the profiles design developed in this research. In the current study, different shroud body length, shroud exit diameter, and various shroud elliptical curve profiles have been studied. The initial dimensionless values of the following parameters with respect to the throat diameter A1, A2, A3 and A4 are 1.05, 1.3, 0.025 and 0.2 respectively.

2.1.3. Shroud geometry equation

The cases studied in this research were axisymmetric about wind turbine axis. Thus, the designed shroud curve will be 2D of revolution and must pass through the three design points: inlet, throat, and exit points (i.e., the function must have solution at these three points). The obtained design curve is revolved around the wind turbine axis. The investigated design curves of the shroud profiles are elliptical curves as shown in Figure 2.

2.2. Mathematical model

In this case, the shroud curve is studied to satisfy the inlet, throat, and exit points, and represent them by general ERE curve equation:

$$\frac{((x-c_1)*cos\alpha-(y-c_2)*sin\alpha)^2}{A^2}+\frac{((x-c_1)*sin\alpha+(y-c_2)*cos\alpha)^2}{B^2}=1 \quad (2)$$

where:
c_1: The x-value for the shifting in the ellipsoid center.
c_2: The y-value for the shifting in the ellipsoid center.
A: The diameter of the ellipsoid on the x-axis.
B: The diameter of the ellipsoid on the y-axis.
α: The rotation angle of the ellipsoid with respect to x-axis.

In order to find the five unknown constants for initial design profile, we should have five specific equations. The coordinates of the inlet point, throat point and exit point are substituted in the general ERE equation. These three points gives only three specific equations i.e., they are not enough to define the general ERE equation. So from the assumption that the minimum value for the shroud curve is located at its intersection with the throat axis line, the derivative of the general ERE equation will be zero.

Now, a set of four equations and five unknowns need to be solved. The rotation angle α is utilized to generate a family of ellipse profiles. Large family of solution is expected at each rotation angle α. The smooth ERE curve which passes through the three points, and match the design constraints is selected. The geometrical design constraint that is imposed on profiles is that their tangent angle at the exit point should be equal or lower than 90 degrees i.e., the profile does not flip back into the flow direction.

2.3. Simulation model

Shear Stress Transport (SST) modeling is chosen. The reason for the selection of SST model is that it represents an improved model from both standard $k-\omega$ model and the transformed $k-\epsilon$ model. This SST model is used in most previous studies and shows very good results that are compatible with experimental results with least error.

In compressible fluids, the flow pattern formation of vortices, and the presence of low pressure regions, have great effect on the performance of shrouded wind turbines. Because all the increment in air mass flow inside the shroud come as a result of vortices formation and low pressure regions presence. So, the flow pattern and flow analysis should be selected correctly in order to obtain results that simulate the real life.

2.3.1. ANSYS meshing

The system is modeled as axisymmetric geometry as shown in Figure 3. The face of the envelope obtained is divided into quadrilateral elements, whereas the inner edge of the target geometry has very fine element compared to far field elements. The mesh is halved in size many times till the variation in the results between successive refinements is less than 0.01%. Figure 4 illustrates the mesh of the system.

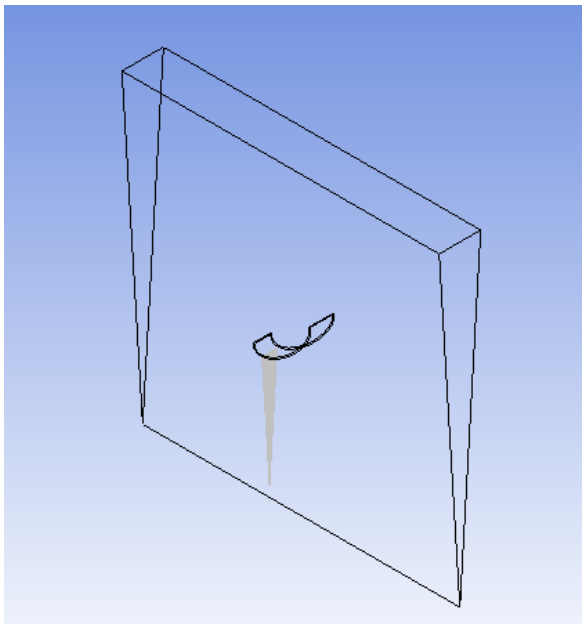

Figure 3. Axisymmetric section of the ANSYS solver.

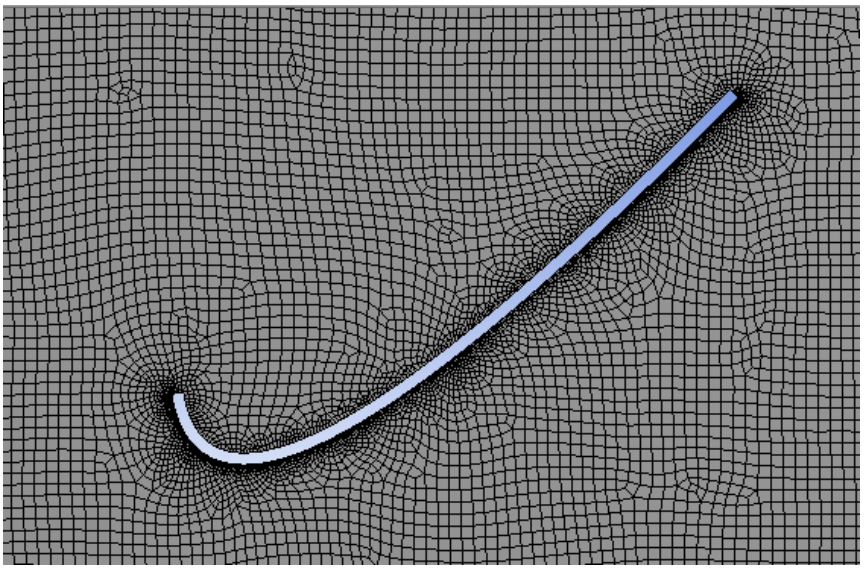

Figure 4. ERE meshing using ANSYS.

2.3.2. Solution setup of ANSYS fluent

The solver is set to pressure-based solver. The velocity formulation is absolute hence the analysis is based on reference value of wind stream velocity. The time selected is steady in order to obtain results of steady state properties of wind flow. The 2D space used is axisymmetric around axis of wind turbine.

The envelope material is chosen to be air with density of 1.225 kg/m³ and viscosity of $1.7894*10^{-5}$ kg/m.s. The inlet velocity is varied in steps 5, 6, 7, 8, 9 and 10 m/s.

For comparison among shroud profiles. The axial wind velocity contours are selected. In order to study the hot (critical) regions around the shroud, and to find the average wind velocity between the axis and shroud for circular section area, the case analysis is set to axisymmetric.

The results show increase of velocity in highest rate near the inner edge of the shroud. The amount of increase in the velocity varies depending on the location with respect to shroud. The size and shape of axial velocity contours varies depending on the shape of the shroud.

Sample of resulting axial velocity contours of ERE profiles at wind velocity 5 m/s is shown in Figure 5.

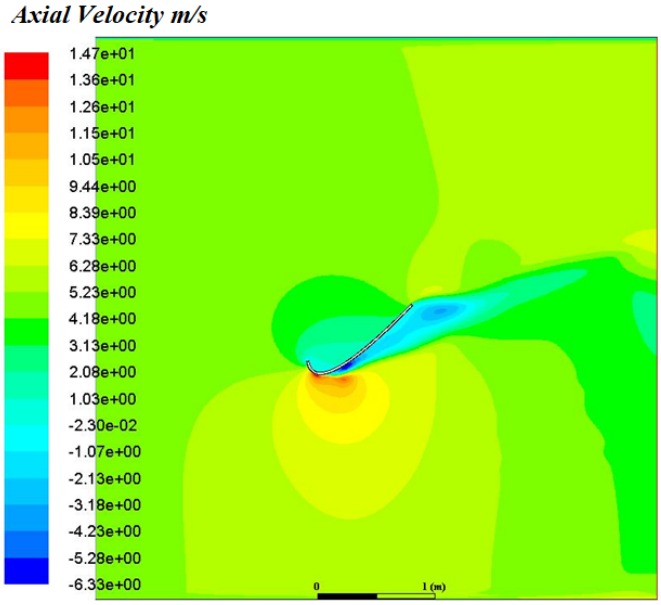

Figure 5. Axial velocity contours for ERE profile at 5 m/s for sample case of angle 0.15π, length ratio 0.10 and diameter ratio 1.3.

2.3.3. Modeling for optimum shroud profile

The shroud profiles are analyzed as an axisymmetric system. The turbine axis has been set as the axis of revolution for the shroud curve. The average wind velocity along the throat section (i.e., turbine blade axis) is considered as the objective of the parametric optimization of the shroud. The search optimization technique is utilized in this research [24].

2.3.4. Solution of ERE profile using different geometry ratios

After solving profiles using the above procedure, the solution of ERE profile for different angle α is performed. To reach the optimum cases the following parameters are varied; body length to throat diameter ratio is varied from 0.1 through 0.3 ratios, exit diameter to throat diameter ratio varied from 1.2 through 1.4 ratios. Noting that the initial ERE is of 0.2 body length ratio, and 1.3 exit diameter ratio i.e., these initial values are the optimum conditions reached by Ohya et al. [9].

The average axial velocity at vertical circular section is compared at shroud throat axis and at different distances from shroud throat axis of 0.1, 0.2, 0.3, 0.4, and 0.5 ratios with respect to diameter. Summary of the optimum profiles for different best angle results at different inlet speeds is presented in Table 1.

Table 1. Summary of optimum shroud profiles.

#	Shape Description	5 m/s	6 m/s	7 m/s	8 m/s	9 m/s	10 m/s	Average ratio
1	0.15 Pi 0.10 Length 1.3 Dia.	1.427	1.435	1.437	1.440	1.441	1.443	1.437
2	0.26 Pi 0.15 Length 1.3 Dia.	1.522	1.525	1.527	1.529	1.531	1.532	1.528
3	0.33 Pi 0.20 Length 1.3 Dia.	1.546	1.548	1.549	1.550	1.550	1.551	1.549
4	0.30 Pi 0.25 Length 1.3 Dia.	1.542	1.544	1.545	1.546	1.546	1.547	1.545
5	0.36 Pi 0.30 Length 1.3 Dia.	1.546	1.548	1.549	1.551	1.551	1.552	1.549
6	0.28 Pi 0.2 length 1.20 Dia.	1.428	1.429	1.429	1.430	1.430	1.430	1.429
7	0.31 Pi 0.2 length 1.25 Dia.	1.486	1.488	1.489	1.490	1.491	1.413	1.476
8	0.23 Pi 0.2 length 1.35 Dia.	1.575	1.577	1.578	1.579	1.580	1.580	1.578
9	0.28 Pi 0.2 length 1.35 Dia.	1.581	1.585	1.586	1.587	1.588	1.588	1.586
10	0.25 Pi 0.2 length 1.40 Dia.	1.611	1.614	1.616	1.618	1.619	1.620	1.616
11	0.26 Pi 0.2 length 1.40 Dia.	1.616	1.620	1.621	1.622	1.623	1.624	1.621

3. Experimental modeling for shroud profile

3.1. Selection of experimental model

The initial ERE profile of 0.2 body length, 1.3 exit diameter ratio and 0.33π (59.4°) rotation angle is one of the best profiles solved among all ratios. This geometrical profile has intermediate variables among all the best profiles; it is the profile selected for experimental validation.

A wind turbine of 500 W was used for the experiment as it is one of the available wind turbines on the market. The turbine rotor diameter is 1030 mm.

3.2. Shroud fabrication

3D printing is utilized in fabricating wind turbine shroud prototype to assure high accuracy profile. Twelve pieces are printed and joined into one complete part. Finishing and coating processes are performed to obtain the final shape of the shroud. Figure 6 shows a photo of the printed shroud. Experimental prototype of the shroud is made of Polylactic Acid material which is a polymer plastic that is used by the 3D printer. The shroud material infill is 15%, where infill is the amount of material that occupies the internal part of the piece. The total mass of the shroud is approximately 2.5 kg.

Figure 6. Shroud assembling process.

3.3. Experimental setup

In the following subsections, the details of the equipment and measurement tools used in conducting the experiments are presented.

3.3.1. Wind generator

The wind generator available in The University of Jordan /Mechanical Engineering Department Laboratory is a low wind speed generator with an open surrounding type. The maximum wind velocity that could be generated using this wind generator is 20 km/hour (about 5 m/s). The dimension of the wind generator output is 1.8 m * 1.8 m. The wind generator used in the experiment is shown in Figure 7a.

3.3.2. Measurement tools and devices used in the experiment:

The main three variables that need to be measured through the experiment are:

1. Distances: the distance between the rotor plane of rotation and the shroud throat axis, the distance between shroud and wind generator exit, … etc. all these distances are measured using traditional meter tape and calipers.
2. Wind velocity: a wireless anemometer device is used to measure the wind velocity in the experiment.
3. Power output: Wattmeter and power analyzer device is used to measure the output of the wind turbine.

The wind generator of the experiment is setup in an open channel field in order to simulate the wind in nature.

The shroud holder is designed to perform the experiment on different distances between the shroud throat plane and wind turbine rotor plane. An external ring is added around the turbine behind the blade axis as illustrated in Figure 7b. The ring is of thin metal bars, to avoid any awkward effect on wind flow around blades.

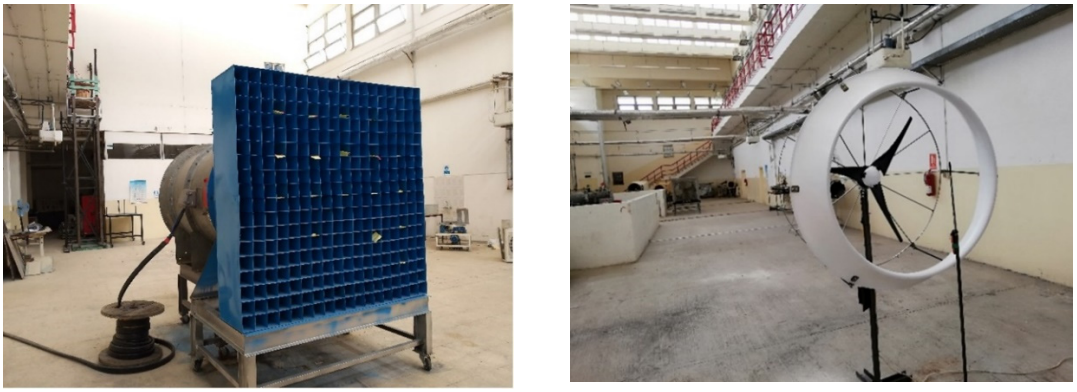

a b

Figure 7. Wind turbine experiment setup.

4. Simulation results

4.1. Shroud curve parameters

The shroud model solved in this work is depending on the equation linking the design parameter is assumed in the initial design of the shroud. The main equation used in the solution is ERE general form.

The comparison between the results is based on the average axial wind velocity developed at the shroud throat axis, and at different distances between the shroud throat axis and the suggested place for the rotor blades plane. These are the main variables affecting the power output of the wind turbine.

All rotation angles that have the solution at the real part of the equation are investigated. The cases solved are for different exit diameter ratios from 1.2 through 1.4, and for cases on body length ratios from 0.1 through 0.3. All cases are solved for the location of the wind turbine from the shroud throat axis.

4.2. Effect of body length ratio

In general, it is found that as the body length increases the average velocity increases to some limit of body length, and then starts decreasing. This effect of body length is related to the vortices formation after shroud body. Also, as the body length increases the vortices formation is increased to some extent. If the body length is increased too much, it will reduce the effect of exit diameter in generating vortices as the streamlines become more parallel to the body. This proves that the body length should be optimized. Sample of the effect of increasing body length ratio, for the case of angle 0.27π, exit diameter at 1.3, and the location is at throat axis, is shown in Figure 8.

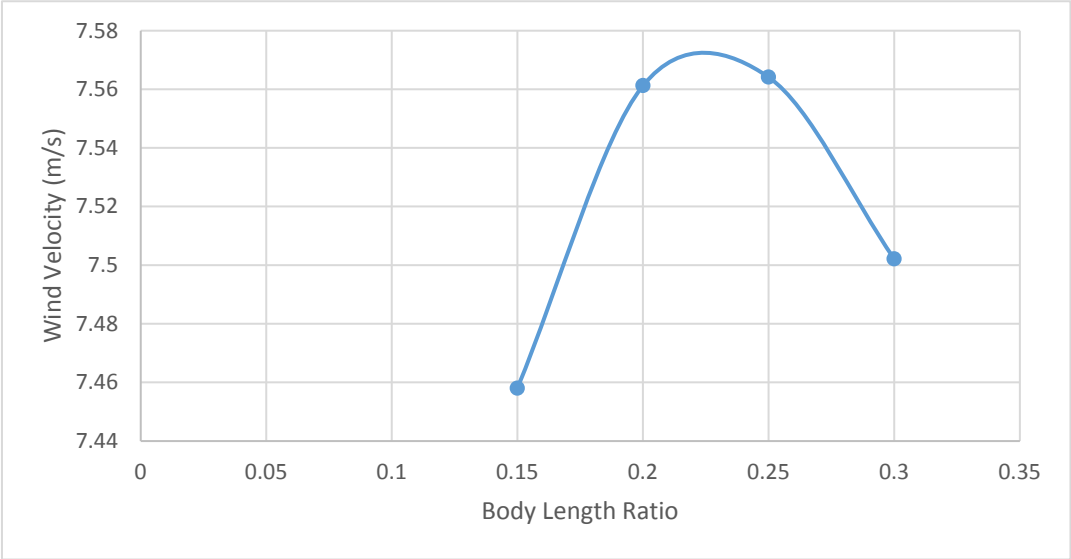

Figure 8. Effect of body length ratio on average wind velocity inside shroud at shroud throat plane.

4.3. Effect of increasing the exit diameter ratio

It is noted that as the exit diameter increases the average velocity and the power output increase. This occurs due to greater changes resulted in streamlines which increase the formation of the vortices behind the shroud. The effect of the exit diameter ratio can be shown in Figure 9. This sample result is shown for the case of body length ratio 0.2, angle 0.33π and diameter ratio 1.2.

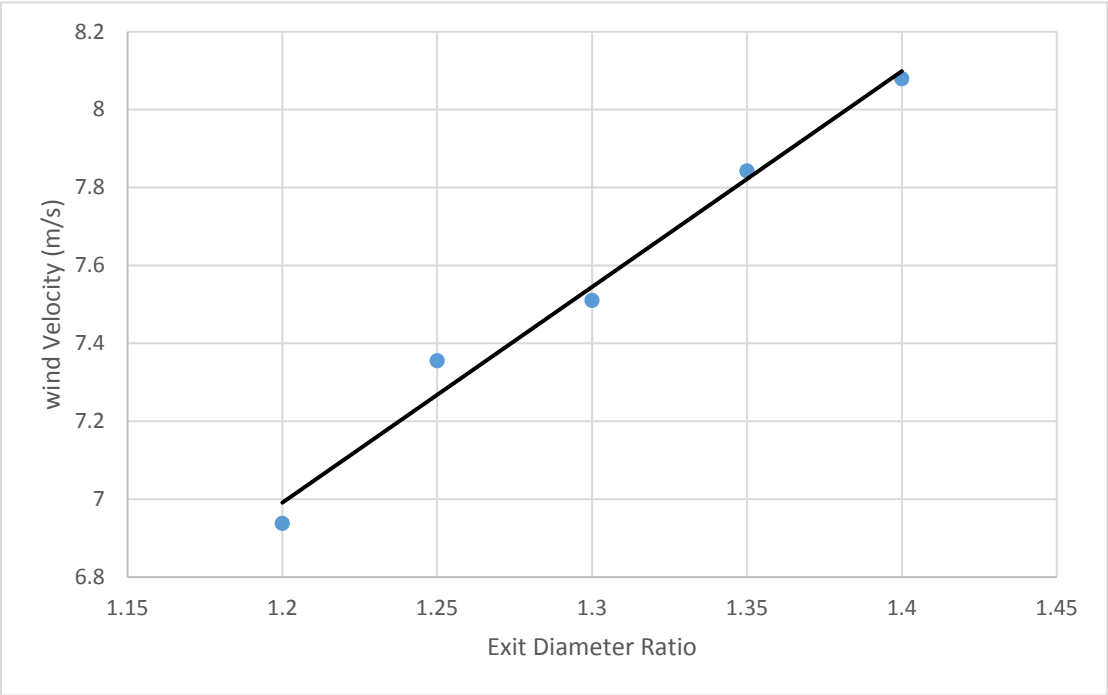

Figure 9. Effect of exit diameter ratio on average wind velocity inside shroud at shroud throat plane.

4.4. Effect of rotation angle

It can be seen from Figure 10 that as the rotation angle increase the average velocity increase, so the power output will increase. The differences at some angles appear due to the shape of the ERE curves. In these curves, the part of ERE curve is smaller and near to straight at certain sections.

The reason of average velocity increase, in most cases when rotation angle increase, is that the shape of the shroud takes a larger segment of the ellipse curve. The effect of rotation angle shown in Figure 10 is a sample result for the case of body length ratio 0.2, exit diameter ratio 1.3 and location at throat axis.

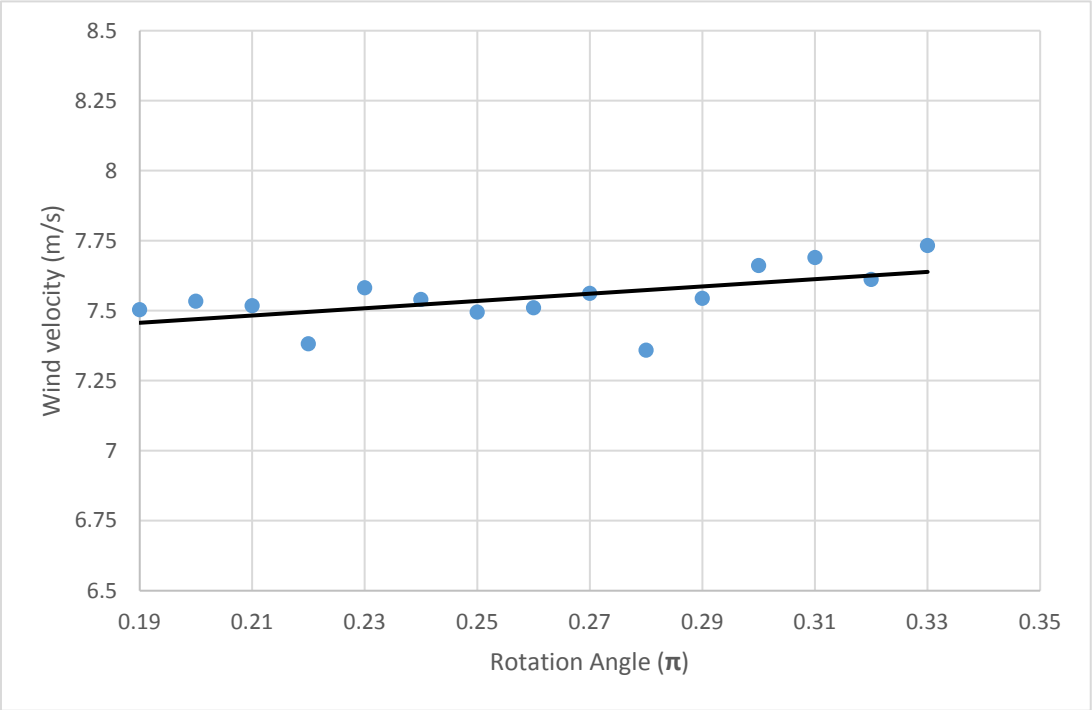

Figure 10. Effect of rotation angle on average wind velocity inside shroud at shroud throat plane.

4.5. Effect of location from shroud throat plane

The location of the wind turbine rotor plane with respect to the shroud throat plane also has main effect on the average wind velocity. As the wind turbine blades axis becomes far from the throat axis, the average wind velocity becomes less. This occurs because the blades become farther from the hot regions (high wind velocity regions) due to the shroud effect. The effect of the location of wind turbine axis with respect to throat axis shown in Figure 11 is sample result for the case of body length ratio of 0.2, exit diameter ratio of 1.3, and rotation angle of 0.33π.

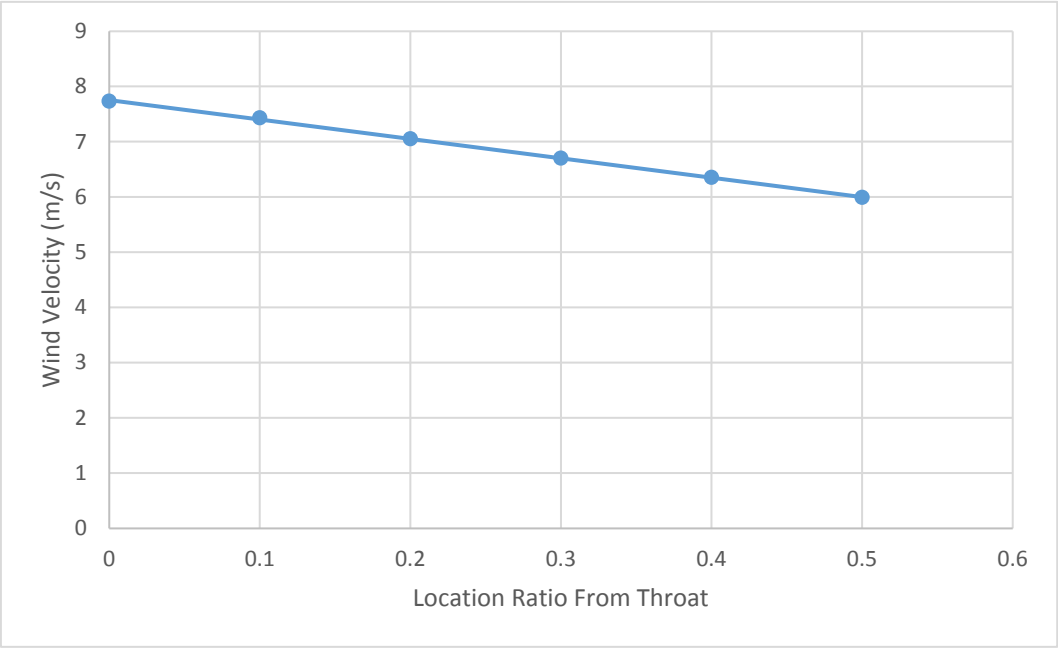

Figure 11. Effect of wind turbine location from shroud throat plane on average wind velocity inside shroud.

4.6. Effect of wind stream velocity

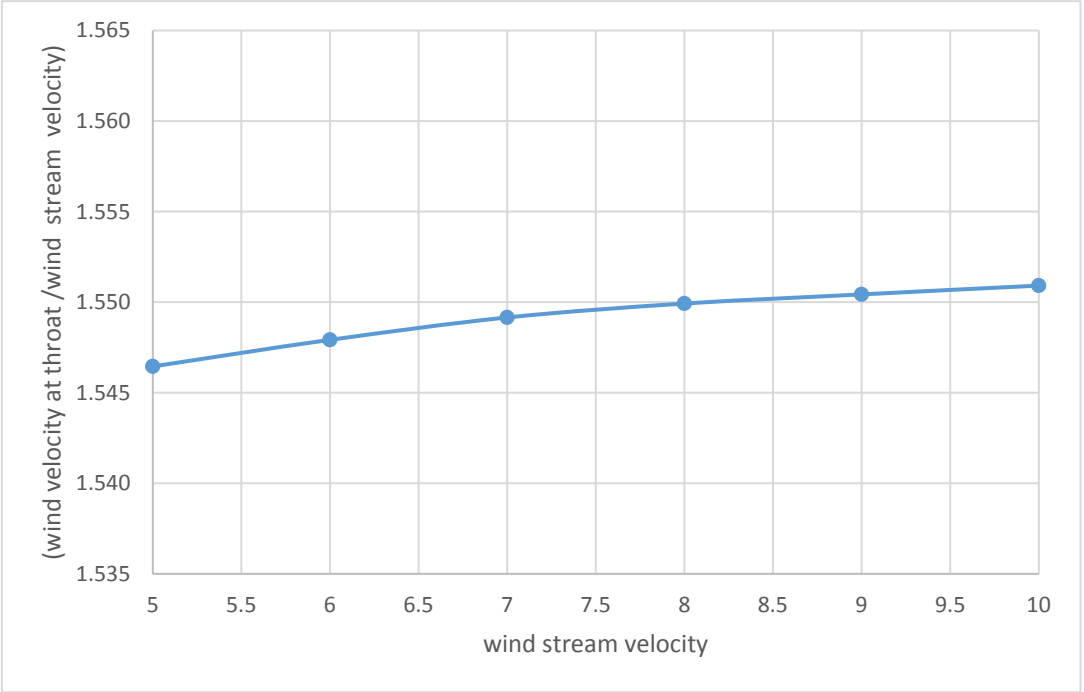

Figure 12. Effect of increasing wind stream velocity on wind velocity ratio inside shroud.

The wind velocity is investigated for velocity ranging from 5 to 10 m/s which is the wind velocity range in Jordan. So the possibility of utilizing obtained shroud in the Jordanian market and on places where the annual wind velocity is close to this average worldwide is explored.

It is noted that as the wind stream velocity increase the ratio of average wind velocity (average wind velocity/wind stream velocity) at the throat axis increase. This occurs due to the increasing effect of the shroud on the vortices formation behind the shroud, i.e., vortices become stronger as velocity increases. The effect of increasing wind stream velocity on wind velocity ratio is shown in Figure 12 for sample case of body length ratio is 0.2, exit diameter ratio 1.3, and the rotation angle 0.33π.

4.7. Results summary of shroud profiles

The results obtained for most cases of shroud profiles show development on average wind velocity ratio (wind stream velocity/average wind velocity) ranging from 1.37 to 1.61 ratio. The proportionality between output power and velocity is to cubic power, i.e., possibility of developing power output in a ratio that exceeds 4 times the power output of the bare wind turbine.

Regarding the maximum wind velocity obtained, most of the cases are near the shroud wall at the throat. It crosses 14 m/s for the wind stream velocity of 5 m/s. The highest value of 16.2 m/s at the throat area is observed for the case of 0.2 body length, 1.4 exit diameter ratio and 0.26π rotation angle as illustrated in Table 1.

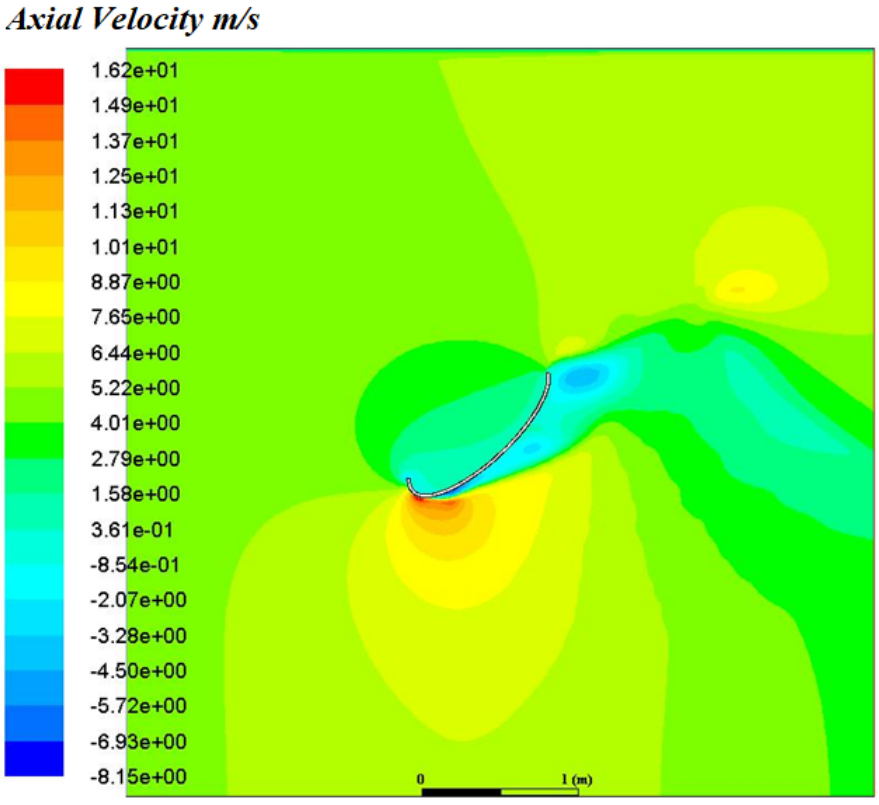

Figure 13. Highest wind velocity obtained at 5 m/s wind stream velocity.

The reason that the maximum wind velocity is recorded near the shroud inner wall at the throat is that the effect of the shroud is maximum on the streamlines at that location. The shroud mouth collects more streamlines and the vortices behind the shroud suck more wind inside the shroud. This forces more streamlines to pass inside the shroud. These streamlines squeezed at the throat area and make the region near the shroud inner wall at the throat have the greatest wind velocity values. The maximum wind velocity is recorded on the throat axis of 0.2 body length ratio, 1.4 exit diameter ratio, and 0.26π rotation angle can be seen in Figure 13. The streamlines for the maximum wind velocity recorded are shown in Figure 14.

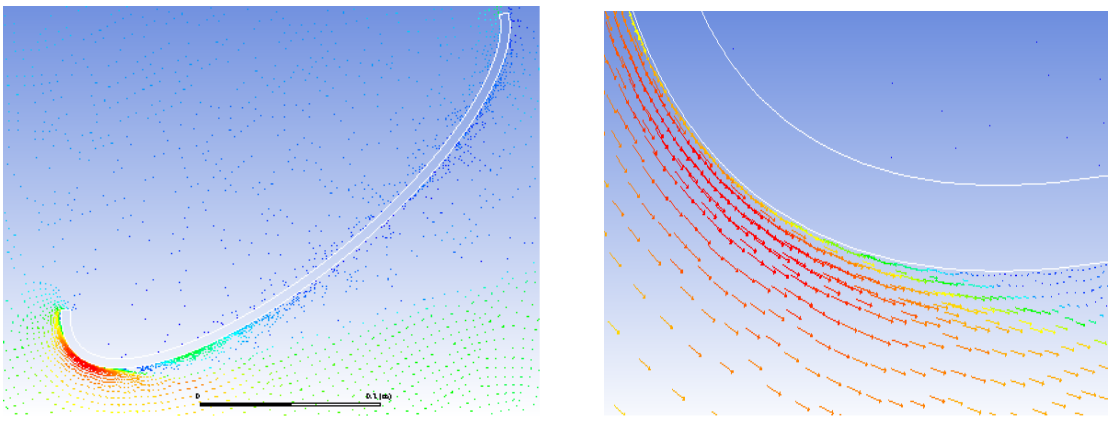

Figure 14. Velocity vectors at wind stream velocity 5 m/s for best shroud profile.

5. Experimental results

An experiment is conducted in order to validate the simulation results obtained from adding shroud to the wind turbine and study the effect of shroud on wind velocity and wind turbine power output, experiments have been performed on bare wind turbine initially, and then on the shrouded wind turbine. The location of the wind turbine is varied with respect to the shroud throat. One of the optimum cases is selected for validating the simulation results.

The model studied in the experiment is 0.2 body length ratio, 1.3 exit diameter ratio, and 0.33π rotation angle of the ellipsoid. The results obtained show a significant increment in wind turbine output power. The effect of the location of the wind turbine blade plane with respect to the shroud throat plane is studied in four tests. The experiment is designed to apply multi-location limits. Due to some limitations in the experiment setup distance ratios 0.0 and 0.1 are not conducted. The experimental results obtained are discussed in the following sections.

5.1. Bare wind turbine results

The experiment has been carried out on a bare wind turbine to study the power output and power factor of the wind turbine under the same boundary conditions of the shrouded wind turbine experiment. The wind stream velocity range for the power generator is limited to 5 m/s. The cut-in

speed of the bare wind turbine is recorded at 3.6 m/s. The relation between wind velocity and output power of bare wind turbine resulted in the experiment can be seen in Figure 15.

In order to compare the experimental results obtained in this study with the results obtained in the simulation part, the power coefficient C_p for the wind turbine used in the experiment has to be calculated. The power coefficient C_p is defined in equation 3 as the ratio between the experimental wind turbine power output obtained to the available power in the wind at the same boundary conditions.

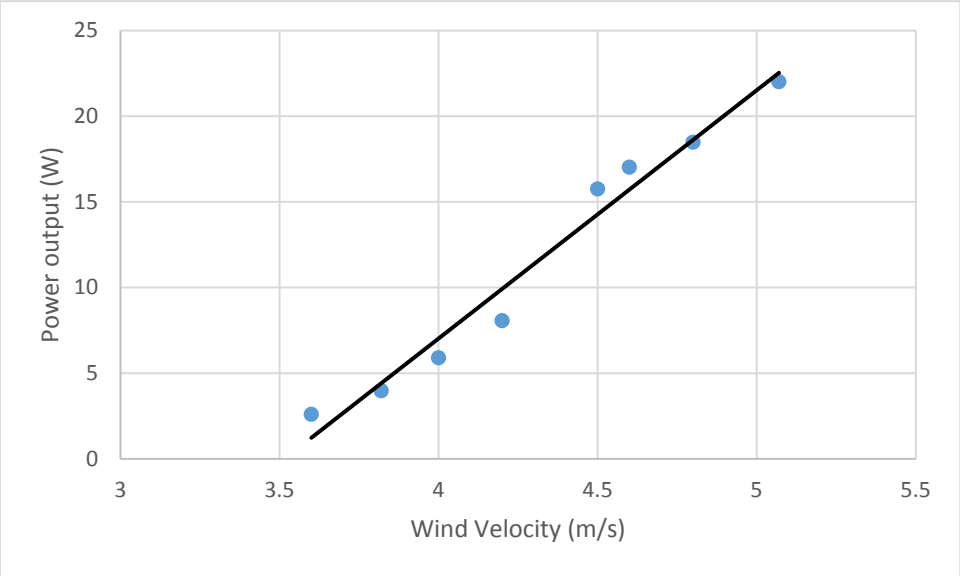

Figure 15. Experimental bare wind turbine power output.

The rotor power coefficient C_p defined as:

$$C_p = \frac{Output\ Power}{Power\ in\ the\ wind} = \frac{P_{out}}{\frac{1}{2}\rho\, A\, U^3} \tag{3}$$

where:
P_{out}: Power output recorded at specific boundary conditions.
ρ: Air density, at it is equal to 1.225 kg/m^3
A: Swept Area of the wind turbine.
U: Wind Velocity.

The diameter of wind turbine (D) used in the experiment is 1.03 meter. The swept area of wind turbine can be calculated as follow:

$$A = \frac{\pi\, D^2}{4}$$

The swept area calculated for our experiment is 0.834 m^2. The wind turbine power coefficient is going to be calculated for different wind velocities carried out in the experiment. The output power for both bare and shrouded wind turbines at wind velocity 5.0 m/s for different turbine locations is summarized in Table 2.

The average power coefficient C_p calculated at 5.0 m/s wind velocity for the wind turbine is 0.335 and this is close to the power factor obtained in Ohya et al. test results of 0.37 [9].

5.2. Shrouded wind turbine results

The model of specification 1.3 length, 0.2 exit diameter, and 0.33π rotation angle of shroud ERE has been tested at 5.0 m/s wind velocity on the following cases: 0.5x, 0.4x, 0.3x, 0.2x meter distance between the blade axis and throat axis where x is the total diameter D_{th}.

The bare wind turbine has been tested at the same wind velocity to compare the test results obtained on shroud cases at the same lab test conditions. The test results obtained are recording the wind stream velocity and the output of the wind turbine (i.e., output Voltage and Ampere) in order to find the output power of the wind turbine in Watts. The tests results obtained for the above four cases and bare wind turbine are shown in Table 2 whereas a comparison between simulation results and experimental results are presented in Table 3. The power output curves obtained for the bare wind turbine, 0.2x, 0.3x, 0.4x, and 0.5x are shown in Figure 16. Also, power coefficient for bare wind turbine and the case of 0.2x are illustrated in Figure 17. The improvement in the power coefficient is very obvious i.e., the rise in the power coefficient is 0.25.

Table 2. Comparison of power output for the bare wind turbine and the shrouded wind turbine at different locations from throat.

#	Wind Velocity	Ampere (Amp)	Volt (V)	Power (W)
bar	5.07	1.68	13.10	22.01
0.2*x*	5.05	2.87	13.52	38.8
0.3*x*	5.05	2.36	13.47	31.79
0.4*x*	5.05	1.77	13.13	23.24
0.5*x*	5.03	1.52	13.04	19.82

*Note: *x* is the total diameter D_{th}.

Table 3. Comparison between the simulation and experimental results.

#	Wind Velocity	Average Power Coefficient C_p	Average wind velocity inside the shroud (Simulation)	Average wind velocity inside the shroud (Experimental)	difference %
bar	5.0	0.335	-	-	
0.2*x*	5.0	0.6	7.05	6.07	13.9
0.3*x*	5.0	0.415	6.70	5.63	15.9
0.4*x*	5.0	0.362	6.35	5.13	19.2
0.5*x*	5.0	0.272	5.99	4.66	22.1

*Note: *x* is the total diameter D_{th}.

The shrouded wind turbine experiment has been performed for four locations of the wind turbine with respect to the throat axis. For each case, the power coefficient is calculated and compared to that obtained for the bare wind turbine. The power coefficient C_p for the bare wind turbine is used to calculate the average wind velocity obtained from adding shroud to the wind turbine. This result is compared with the simulation wind velocity developed from adding the shroud.

The boundary conditions for the shrouded wind turbine are the same as that in bare wind turbine experiment; the air density is 1.225 kg/m^3, the swept area is calculated to be 0.834 m^2. The power coefficient C_p for the shrouded wind turbine at four locations of the wind turbine blade axis to the throat axis has been calculated. The results obtained in those four cases are summarized in Table 3. The experimental column in Table 3 is calculated based on the data obtained from the experiment.

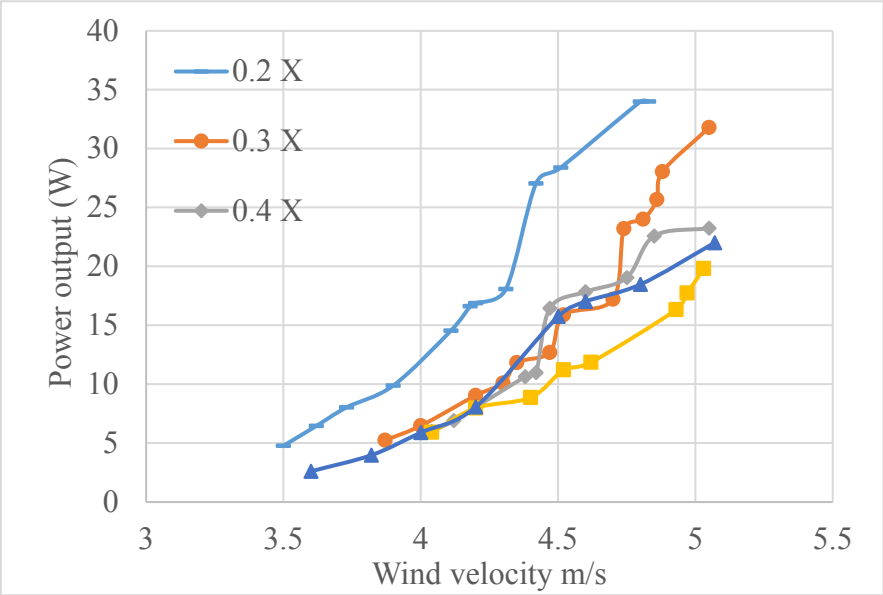

Figure 16. Power output curves.

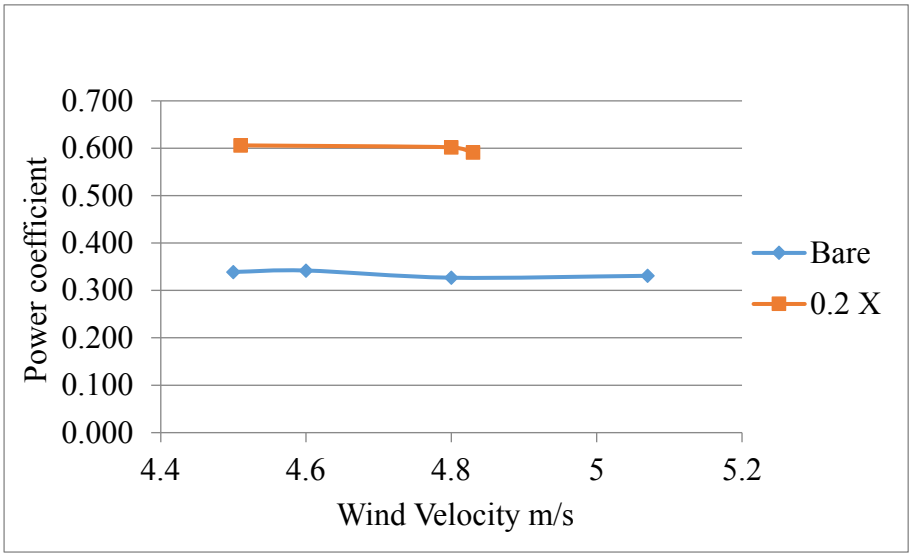

Figure 17. Power coefficient for bare turbine and shrouded at location of 0.2X.

The average power coefficient calculated is 0.6 which slightly exceed Betz limit of 0.59 and this proofs that Betz limit is only valid for bare wind turbine where the effect of vortices formulation is absent. This improvement in power coefficient for the wind turbine from 0.335 for the bare wind turbine to 0.6 for the shrouded wind turbine is a considerable achievement.

The experiment is performed in open tunnel conditions whereas in the simulation it is assumed as a large close tunnel. It can be noted from Table 3 that as the wind turbine blade axis is located farther from the throat axis, the difference between the simulation results and experimental results increase. This is due to the increase of vortices formation at the shroud entrance where wind speed is measured.

5.3. Shrouded wind turbine best profile

The best profile obtained in the simulation is of 0.2 body length ratio, 1.4 exit diameter ratio, and 0.26π rotation angle and location at the throat axis. The average equivalent wind velocity increase ratio is calculated for wind stream velocity of 5 m/s. This profile shows a development in wind speed of 1.621 times the wind stream velocity, i.e., the average wind velocity inside the shroud is calculated to be 8.08 m/s. Using the bare wind turbine which has power coefficient C_p of 0.335 in the experiment, when shrouded the wind turbine supposed to generate 90.24 W compared to 21.39 W for the bare wind turbine case. This leads to a power improvement of 4.22 times compared to the bare wind turbine on ideal conditions.

The best profile is not used because the shroud size couldn't be fabricated using the available 3D printer. The profile fabricated is of 0.2 body length ratio, 1.3 exit diameter ratio and 0.33π rotation angle. The calculated average wind velocity inside the shroud is 7.73 m/s for wind stream 5 m/s for the turbine location at the throat. The wind turbine utilized in the experiment has power coefficient C_p of 0.335. When it is shrouded the wind turbine should generate 79.10 W compared to 21.39 W for the bare wind turbine case. This means that the improvement in the output power is 3.7 times of the bare wind turbine.

5.4. Shroud approximate cost calculation

Simple approximate cost calculation for the shroud made of reinforced composite material. The material selected is fiber glass composite material since it is cheap and available. Table 4 shows cost calculations that is carried for 100 shrouds. The shroud cost is 64$, which very good compared to the power improvement.

Table 4. Approximate cost calculation for shroud Fabrication from fiber glass reinforced material

Item	Cost $/unit	Cost 100 pieces ($)
Total area of needed of fiber glass per piece: 1.8 m^3	10 $/m	1800
Wood Mold	1000 $/Mold	1000
Labor cost for 2 hours of work per piece	10 $/hour	2000
Utilities per piece	8 $/Piece	800
miscellaneous	8 $/Piece	800
Total Cost for 100 piece (shrouds)		6400
Approximate Cost of one shroud		64

6. Conclusions

The mathematical analysis of different elliptical shroud profiles is carried out. Open tunnel experiment for one of the best shroud profiles is performed. The mathematical, simulation and experimental analysis are carried out to present the effect of the shroud profile parameters on wind velocity inside the shroud. The profiles analyzed mathematically are those that have real solutions for the elliptical equation and their tangent angle at the exit point is equal or lower than 90 degrees i.e., the profile does not flip back into the flow direction. All profiles that pass the design criterion achieve an average axial velocity increase in the range of 1.37 to 1.62 times the wind stream velocity. The results demonstrates that the geometrical parameters affect the average axial wind velocity at different levels. The exit diameter of the shroud is the most effective parameter in

improving the wind turbine performance, whereas the shroud body length increases the wind velocity inside the shroud to a certain extent.

The experimental results show very good agreement with the simulation results. The experiment has proved that the shrouded wind turbine exceeds the Betz limit i.e., the Betz limit is only valid for bare wind turbines.

Conflict of interest

The authors declare no conflict of interest.

References

1. Vries O (1979) Fluid dynamic aspects of wind energy conversion. North Atlantic Treaty Organization Advisory Group for Aerospace Research and Development, Neuilly-sur-Seine France.
2. Bontempo R, Manna M (2016) Effects of the duct thrust on the performance of ducted wind turbines. *Energy* 99: 274–287.
3. Bontempo R, Manna M (2020) On the potential of the ideal diffuser augmented wind turbine: an investigation by means of a momentum theory approach and of a free-wake ring-vortex actuator disk model. *Energy Convers Manage* 213: 112794.
4. Avallone F, Ragni D, Casalino D (2020) On the effect of the tip-clearance ratio on the aeroacoustics of a diffuser-augmented wind turbine. *Renewable Energy* 152: 1317–1327.
5. Dighe VV, de Oliveira G, Avallone F, et al. (2019) Characterization of aerodynamic performance of ducted wind turbines: A numerical study. *Wind Energy* 22: 1655–1666.
6. Venters R, Helenbrook BT, Visser KD (2018) Ducted Wind Turbine Optimization. *J Sol Energy Eng* 140: 011005.
7. Bontempo R, Manna M (2020) Diffuser augmented wind turbines: Review and assessment of theoretical models. *Appl Energy* 280: 115867.
8. Ohya Y, Karasudani T, Sakurai A, et al. (2008) Development of a shrouded wind turbine with a flanged diffuser. *J Wind Eng Ind Aerodyn* 96: 524–539.
9. Ohya Y, Karasudani T (2010) A shrouded wind turbine generating high output power with wind-lens technology. *Energies* 3: 634–649.
10. Srikanth SK (2016) Numerical analysis of wind lens. *Int J Innov Res Sci Eng Technol*, 5.
11. Takahashi S, Hata Y, Ohya Y, et al. (2012) Behavior of the blade tip vortices of a wind turbine equipped with a brimmed-diffuser shroud. *Energies* 5: 5229–5242.
12. Kosasih B, Tondelli A (2012) Experimental study of shrouded micro-wind turbine. *Procedia Eng* 49: 92–98.
13. Toshimitsu K, Kikugawa H, Sato K, et al. (2012) Experimental investigation of performance of the wind turbine with the flanged-diffuser shroud in sinusoidally oscillating and fluctuating velocity flows. *Open J Fluid Dyn* 2: 215–221.
14. Govindharajan R, Parammasivam KM, Vivel V, et al. (2013) Numerical investigation and design optimization of brimmed diffuser—Wind lens around a wind turbine. *Eighth Asia-Pacific Conference on Wind Engineering*, 1204–1210.

15. Jafari SAH, Kosasih B (2014) Flow analysis of shrouded small wind turbine with a simple frustum diffuser with computational fluid dynamics simulations. *J Wind Eng Ind Aerodyn* 125: 102–110.
16. Kosasih BY, Jafari SA (2014) High-Efficiency shrouded micro wind turbine for urban-built environment. *Appl Mech Mater* 493: 294–299.
17. Maia LAB Experimental and numerical study of a diffuser augmented wind turbine—DAWT. Master thesis, 2014. Available from: https://bibliotecadigital.ipb.pt/handle/10198/11600.
18. Sangoor AJ (2015) Experimental and computational study of the performance of a new shroud design for an axial wind turbine. Available from: https://etd.ohiolink.edu/apexprod/rws_olink/r/1501/10?clear=10&p10_accession_num=ysu1433503872.
19. Liu J, Song M, Chen K, et al. (2016) An optimization methodology for wind lens profile using Computational Fluid Dynamics simulation. *Energy* 109: 602–611.
20. Jenkins PE, Younis A, Jenkins PE, et al. (2016) Flow simulation to determine the effects of shrouds on the performance of wind turbines. *J Power Energy Eng* 4: 79–93.
21. Oka N, Furukawa M, Kawamitsu K, et al. (2016) Optimum aerodynamic design for wind-lens turbine. *J Fluid Sci Technol* 11: JFST0011–JFST0011.
22. El-Zahaby AM, Kabeel AE, Elsayed SS, et al. (2017) CFD analysis of flow fields for shrouded wind turbine's diffuser model with different flange angles. *Alexandria Eng J* 56: 171–179.
23. Ohya Y, Karasudani T, Nagai T, et al. (2017) Wind lens technology and its application to wind and water turbine and beyond. *Renewable Energy Environ Sustainability* 2: 2.
24. Chapra S, Canale R (2006) Numerical Methods for Engineers, McGraw-Hill. 6 Eds, New York: McGraw-Hill.

AIMS Press